# Cellular heterogeneity in pressure and growth emerges from tissue topology and geometry

Yuchen Long[1,*], Ibrahim Cheddadi[2,3], Vincent Mirabet[1], Mathilde Dumond[1,4], Christophe Godin[1,2], Arezki Boudaoud[1,*].

1. Laboratoire Reproduction et Développement des Plantes, Univ Lyon, ENS de Lyon, UCB Lyon 1, CNRS, INRA, INRIA, F-69342, Lyon, France.

2. INRIA/CIRAD/INRA Project-team Virtual Plants, France.

3. Current address: Laboratoire TIMC-IMAG/DyCTiM, Université Grenoble Alpes, CNRS, UMR 5525, 38706 La Tronche, France.

4. Current address: Department of Biosystems Science and Engineering, ETH Zurich, Mattenstrasse 26, 4058, Basel, Switzerland.

*. Correspondence should be addressed to yuchen.long@ens-lyon.fr or arezki.boudaoud@ens-lyon.fr

## Abstract

Cell-to-cell heterogeneity prevails in many biological systems, although its origin and function are often unclear. Hydrostatic pressure, alias turgor pressure, is an essential cellular property in tissue physiology and morphogenesis, and its spatial variations are often overlooked. Here, using atomic force microscopy, we demonstrate that hydrostatic pressure is highly heterogeneous in the epidermis of Arabidopsis shoot apical meristem, and it unexpectedly correlates either positively or negatively with cellular growth rate, depending on growth conditions. Combining experimental arguments and computational modeling of cell wall mechanics and osmosis within multicellular tissues, we show that pressure and growth heterogeneities emerge jointly from cell size and topology. Our results suggest that growth and pressure heterogeneities are intrinsic properties in compact tissues with inhomogeneous topology.

## One sentence summary

Tissue geometry and topology prescribe heterogeneity in hydrostatic pressure and growth.

**Key words**

Cellular heterogeneity, hydrostatic pressure, tissue topology, growth mechanics, atomic force microscopy, mechanical modeling.

**Main text**

Within a cell population of same genetic origin, cellular heterogeneity can be observed for many characteristics like gene expression, signal perception and shape changes including growth (*1*). Decades of studies have identified numerous stochastic or deterministic cellular variations in different biological systems (*1–4*) that may trigger diverging cellular responses, phenotypically segregating distinct cell subpopulations (*5–8*), yet the origin and implication of most heterogeneous properties remain elusive.

Recent studies highlight that, within a tissue, cell growth rate can be highly heterogeneous, a phenomenon which impacts tissue patterning and macroscopic growth robustness (*1*, *2*). Cell volume changes are partially due to osmosis (*9–11*), and walled cells in plants, bacteria and fungi can sustain large cross-membrane osmotic potential differences by accumulating hydrostatic pressure, alias turgor pressure, greater than atmospheric pressure (Fig. S1) (*12*). Although less prominent, animal cells also accumulate hydrostatic pressure, especially when compacted or contracting (*13*, *14*). In plants, it is believed that turgor pressure positively correlates with growth rate, as depicted in the Lockhart-Ortega equation (Fig. S1) (*15*). However, observations suggest that growth rate and pressure level are not always associated (*16*), challenging the link between growth regulation and cellular pressure buildup.

Recent advances in atomic force microscopy (AFM) enabled non-invasive turgor pressure measurement utilizing indentation force-displacement and surface topography in living plant cells (Fig. 1A) (*17*). Here, we took advantage of these advances and assessed the relation between cell-specific turgor pressure and growth in the epidermis of the *Arabidopsis thaliana* shoot apical meristem (SAM), a system that features substantial growth heterogeneity (*1*).

In SAM co-treated with naphthylphthalamic acid (NPA) and oryzalin, a polar auxin transport inhibitor that induces pin-formed SAM and a microtubule-depolymerizing drug that blocks cell division but permits continuous, isotropic growth, the often curved cell walls suggest that neighboring cells have different turgor pressure (*18*). Cell-specific AFM measurements on nine SAMs revealed that turgor pressure is markedly heterogeneous in oryzalin-treated SAM epidermis (Fig. 1E). Each SAM had a different average turgor pressure (Fig. S2), consistent with previous report (*19*). This however complicates the comparison of pressure heterogeneity between SAMs. Thus, we normalized cellular turgor pressure to the average pressure per individual SAM. Closer inspection revealed that normalized turgor pressure anticorrelates with the number of cell-neighbors in the epidermis, i.e. cells with fewer epidermal neighbors have higher turgor pressure, with 1.4-fold difference between four and eight-neighbored cells ($n$ = 202 cells, Pearson correlation coefficient $R$ = -0.34, $p < 10^{-6}$) (Fig. 1F), consistent with previous prediction (*18*). In dividing, untreated SAMs, we also detected similar turgor-neighbor number anticorrelation (5 SAMs, $n$ = 326 cells, $R$ = -0.16, $p$ = 0.004) (Fig. 1G-J) both in central zone and peripheral zone (Fig. S3), confirming that nonrandom turgor pressure heterogeneity can robustly establish in tissues with static topology (no neighbor number change) or dynamic topology (neighbor number changes due to division). Thus, turgor pressure heterogeneity associates with local tissue topology.

Earlier works suggesting cellular pressure heterogeneity (*18*, *20*) simply treated hydrostatic pressure as a biased input or required differential osmotic pressure. To further explore and explain the topological association of turgor pressure variability in SAMs, we constructed a 2D vertex model with topological distribution similar to SAM (Fig. S4) attributing turgor buildup and water flow through the tissue to osmosis (Cheddadi et al. unpublished) (Fig. 2A). The model is similar to the Lockhart-Ortega equation of visco-elasto-plastic growth of a single cell (Fig. S1) (*15*), with the important difference that we consider a multicellular tissue with more realistic 2D polygonal geometry. Cell wall growth is akin to visco-plastic flow (irreversible deformation) and occurs when elastic strain (reversible deformation) induced by turgor pressure is greater than a threshold (Fig. 2A). Water influx is driven by the cross-membrane water potential difference, and turgor-driven intercellular water

redistribution is allowed via plant plasmodesmata (*21*), which play overlapping roles as gap junctions or cytoplasmic bridges in animals (*22*, *23*). We did not prescribe turgor pressure, instead letting it emerge from local mechanical and hydraulic interplays. Surprisingly, even with homogenous cellular parameters (i.e. cellular osmotic potential, cross-membrane and intercellular water conductivities, cell wall elasticity, extensibility and strain threshold), we could recover the turgor-neighbor number anticorrelation in our model similar to experimental measurements, without or with cell divisions to mimic oryzalin-treated or untreated SAM, respectively (no division 5 simulations, n = 1219 cells, $R$ = -0.87, $p = 10^{-100}$; dividing 8 simulations, $n$ = 3240 cells, $R$ = -0.58, $p = 10^{-100}$) (Fig. 2B-G). This implies that local hydrostatic pressure heterogeneity does not require differential cellular osmotic pressure (*18*), and predicts a topological origin of pressure variability.

In SAM surface, cell neighbor number and size are coupled (Fig. S4). Consistently, cell-specific turgor pressure also anticorrelates with normalized cell area (Fig. S4). To further explore turgor's association with local topology and cell size, we modified the initial state of our simulation to have four-neighbored cells bigger than eight-neighbored cells, and found that higher turgor pressure accumulated in four-neighbored cells and not in the smaller eight-neighbored cells (Fig. S4). This confirms that turgor pressure heterogeneity emerges from tissue topology rather than cell size differences. Such phenomenon can be explained by local topology, which determines the cell wall angles and the subsequent cell wall tension distribution at each three-cell junction (Fig. 2H-K): in our model, due to wall rheology and hydraulic limitations, elastic strain (relative deformation) and stress (tension) are capped slightly above the growth–threshold, and are almost homogeneous in the whole tissue. Therefore, the sum of wall tension at each three-cell junction (vertex) depends only on the angles between walls. The vertex between three hexagonal cells with 120 ° internal angles has a sum of tension at 0 (Fig. 2H, I). Fewer-neighbored cells have sharper internal angles, so the sum of tension at vertex is greater towards the cell interior, effectively creating additional inward compression and prompting higher turgor pressure buildup at equilibrium (Fig. 2J, K). Since topology is highly conserved between tissue contexts in many biological systems (*24*), we propose that hydrostatic pressure heterogeneity is an innate characteristic of any compact

tissue with polygonal cells (*25*), which adjusts itself to reconcile local mechanical and hydraulic conditions.

In SAM, cellular growth rate is known to be heterogeneous (*1*). To assess the relation between turgor and growth heterogeneity, we monitored areal growth rate of SAM epidermal cells per topological category by time-lapse confocal microscopy. Untreated SAMs exhibited anticorrelation of cell growth rate with neighbor number (11 SAMs, $n$ = 2013 cells, $R$ = -0.13, $p < 10^{-8}$; Fig. 3E) and cell size (Fig. 3F; $R$ = -0.28, $p < 10^{-36}$). Our observations support previous reports that smaller cells in SAM tend to grow faster (*1*), and suggests that higher turgor pressure in fewer-neighbored cells associates with faster growth. Unexpectedly, in oryzalin-treated SAMs, the fewer-neighbored and small cells grew slower (14 SAMs, $n$ = 1160 cells; Fig. 3K, neighbor number $R$ = 0.14, $p < 10^{-5}$; Fig. 3L, cell size $R$ = 0.22, $p = 10^{-14}$). This suggests that higher turgor pressure associates with either faster or slower growth depending on conditions (Fig. S4). Although seemingly a small shift, this negative-to-positive slope change of local growth heterogeneity captures a strong qualitative inversion of growth behavior (Fig. 3D, J), where relative cell size increases exponentially in opposite fashions (Fig. S5).

Next, we explored the potential origin of growth variability with our computational model. Nonrandom growth heterogeneity emerged from our model with homogenous parametric inputs, similar to turgor pressure buildup, with the smaller, fewer-neighbored cells growing faster (8 simulations, $n$ = 3240 cells; $G$ vs $N$, $R$ = -0.05, $p$ = 0.002, Fig. 4B; $G$ vs $S$, $R$ = -0.82, $p < 10^{-100}$) that recapitulates the untreated SAM (Fig. 3A-F). We then attempted to mimic oryzalin-treated SAM by blocking cell division in the model, but found it not sufficient to invert the topology-growth trend (Fig. 4D-F), indicating that additional parameter changes are needed to recapitulate oryzalin-treated growth heterogeneity.

Our model predicts two antagonistic phenomena that impact growth: growth rate depends on the access to water resource which flows across cell surface, so smaller cells benefit from a higher surface-versus-volume ratio for relatively more water influx and volume increase; meanwhile, the often-smaller fewer-neighbored cells are under extra mechanical compression

due to tissue topology (Fig. 2K) and would grow slower. Therefore, since the often-smaller fewer-neighbored cells grow faster in untreated meristems, the model suggests that the flux limitation is predominant in this condition, while oryzalin treatment elevates the relative importance of the mechanical limitation. We explored the parameter space of the model, and found that raising strain threshold or decreasing osmotic pressure can elevate the predominance of mechanical constraint (Fig. 4G-L), effectively switches the system from cell-size-and-flux-controlling to topology-and-mechanic-controlling (Fig. S6).

Interestingly, our models that exhibited untreated SAM growth trends have growth rate correlated better with cell size than neighbor number (Fig. 4A-F), while models recapitulating oryzalin-treated growth trends correlated better with cell neighbor number than size (Fig. 4G-L). We tested this in experiments, focusing on the slope of growth rate against neighbor number or cell size, and found that the level of growth heterogeneity in individual SAMs correlates with average SAM growth rate (Fig. S6): topology-associated growth heterogeneity is stronger in fast-growing oryzalin-treated SAMs ($n$ = 14 SAMs, $R$ = 0.63, $p$ = 0.02 < 0.05), while size-associated growth heterogeneity is stronger in slow-growing untreated SAMs ($n$ = 11 SAMs, $R$ = 0.68, $p$ = 0.02 < 0.05) (Fig. S6). No significant correlation of size-associated growth heterogeneity was found in oryzalin-treated SAMs ($R$ = 0.14, $p$ = 0.53 > 0.05), neither topology-associated correlation in untreated SAMs ($R$ = 0.56, $p$ = 0.07 > 0.05). This indicates that growth heterogeneity is more sensitive to size-related properties in untreated SAMs, or to topology-related properties in oryzalin-treated SAMs, as predicted by the model. Furthermore, it shows that growth heterogeneity scales with global growth speed, where faster growth enhances the cell size amplifying effect of oryzalin treatment, and reduces the cell size homogenizing tendency in untreated scenario (Fig. S6). This suggests that faster tissue growth favors enhanced cell size variability.

Together, we demonstrate that cellular hydrostatic pressure is innately heterogeneous in Arabidopsis SAM epidermis, however it is not a proxy of local growth rate variability, as previously believed. Instead, growth rate and turgor pressure are combinatorial outputs of local mechanics and hydraulics, which in part emerge from local topology and cell size, respectively. Each of these parameters may be controlled by genetic and biochemical inputs,

and small changes in these biological inputs may potentially enable drastic shifts of cell size distribution (Fig. S6). A growth variability switch is observed for example during sepal development, where smaller and often fewer-neighbored cells grow faster in young sepals then slower in older sepals, effectively switching from homogenizing to amplifying cell size variability (*26*). The emergent heterogeneity of local growth and hydrostatic pressure likely underlies morphogenesis in other compact tissues with polygonal cells.

**Acknowledgements**

We thank L. Beauzamy for AFM training. This work was supported by a fellowship from Institut Universitaire de France and an ERC Starting Grant "PhyMorph" to A.B. (ERC-2012-StG-307387), an EMBO Long-term Fellowship to Y.L. (EMBO ALTF 168-2015), and an Agropolis Fundation grant (MecaFruit3D) to I.C. and C.G..

**References**

1. L. Hong *et al.*, Heterogeneity and Robustness in Plant Morphogenesis: From Cells to Organs. *Annu. Rev. Plant Biol.* **69**, 469–495 (2018).

2. K. Kamimoto *et al.*, Heterogeneity and stochastic growth regulation of biliary epithelial cells dictate dynamic epithelial tissue remodeling. *eLife*. **5** (2016), doi:10.7554/eLife.15034.

3. R. Ietswaart, S. Rosa, Z. Wu, C. Dean, M. Howard, Cell-Size-Dependent Transcription of FLC and Its Antisense Long Non-coding RNA COOLAIR Explain Cell-to-Cell Expression Variation. *Cell Syst.* **4**, 622-635.e9 (2017).

4. Y. Long *et al.*, In vivo FRET-FLIM reveals cell-type-specific protein interactions in Arabidopsis roots. *Nature*. **548**, 97–102 (2017).

5. A. Eldar, M. B. Elowitz, Functional roles for noise in genetic circuits. *Nature*. **467**, 167–173 (2010).

6. J. R. Chubb, Symmetry breaking in development and stochastic gene expression. *Wiley Interdiscip. Rev. Dev. Biol.* **6**, e284 (2017).

7. G. Donati, F. M. Watt, Stem Cell Heterogeneity and Plasticity in Epithelia. *Cell Stem Cell*. **16**, 465–476 (2015).

8. M. J. Gerdes *et al.*, Emerging Understanding of Multiscale Tumor Heterogeneity. *Front. Oncol.* **4** (2014), doi:10.3389/fonc.2014.00366.

9. K. Watanabe, T. Umeda, K. Niwa, I. Naguro, H. Ichijo, A PP6-ASK3 Module Coordinates the Bidirectional Cell Volume Regulation under Osmotic Stress. *Cell Rep.* **22**, 2809–2817 (2018).

10. K. Xie, Y. Yang, H. Jiang, Controlling Cellular Volume via Mechanical and Physical Properties of Substrate. *Biophys. J.* **114**, 675–687 (2018).

11. M. Guo *et al.*, Cell volume change through water efflux impacts cell stiffness and stem cell fate. *Proc. Natl. Acad. Sci.* **114**, E8618–E8627 (2017).

12. J. Dumais, Y. Forterre, "Vegetable Dynamicks": The Role of Water in Plant Movements. *Annu. Rev. Fluid Mech.* **44**, 453–478 (2012).

13. M. P. Stewart *et al.*, Hydrostatic pressure and the actomyosin cortex drive mitotic cell rounding. *Nature*. **469**, 226–230 (2011).

14. F. Montel *et al.*, Stress clamp experiments on multicellular tumor spheroids. *Phys. Rev. Lett.* **107**, 188102 (2011).

15. J. K. Ortega, Augmented growth equation for cell wall expansion. *Plant Physiol.* **79**, 318–320 (1985).

16. J. H. Kroeger, R. Zerzour, A. Geitmann, Regulator or driving force? The role of turgor pressure in oscillatory plant cell growth. *PloS One*. **6**, e18549 (2011).

17. L. Beauzamy, J. Derr, A. Boudaoud, Quantifying Hydrostatic Pressure in Plant Cells by Using Indentation with an Atomic Force Microscope. *Biophys. J.* **108**, 2448–2456 (2015).

18. F. Corson *et al.*, Turning a plant tissue into a living cell froth through isotropic growth. *Proc. Natl. Acad. Sci. U. S. A.* **106**, 8453–8458 (2009).

19. L. Beauzamy, M. Louveaux, O. Hamant, A. Boudaoud, Mechanically, the Shoot Apical Meristem of Arabidopsis Behaves like a Shell Inflated by a Pressure of About 1 MPa. *Front. Plant Sci.* **6** (2015), doi:10.3389/fpls.2015.01038.

20. S. Ishihara *et al.*, Comparative study of non-invasive force and stress inference methods in tissue. *Eur. Phys. J. E Soft Matter*. **36**, 9859 (2013).

21. W. J. Lucas, B.-K. Ham, J.-Y. Kim, Plasmodesmata - bridging the gap between neighboring plant cells. *Trends Cell Biol.* **19**, 495–503 (2009).

22. N. M. Kumar, N. B. Gilula, The Gap Junction Communication Channel. *Cell*. **84**, 381–388 (1996).

23. P. F. McLean, L. Cooley, Protein Equilibration through Somatic Ring Canals in Drosophila. *Science*. **340** (2013), doi:10.1126/science.1234887.

24. W. T. Gibson, M. C. Gibson, in *Current Topics in Developmental Biology* (Academic Press,

2009; http://www.sciencedirect.com/science/article/pii/S0070215309890042), vol. 89 of *Current Topics in Developmental Biology*, pp. 87–114.

25. B. Péret *et al.*, Auxin regulates aquaporin function to facilitate lateral root emergence. *Nat. Cell Biol.* **14**, 991–998 (2012).

26. S. Tsugawa *et al.*, Clones of cells switch from reduction to enhancement of size variability in Arabidopsis sepals. *Development*. **144**, 4398–4405 (2017).

## Figures

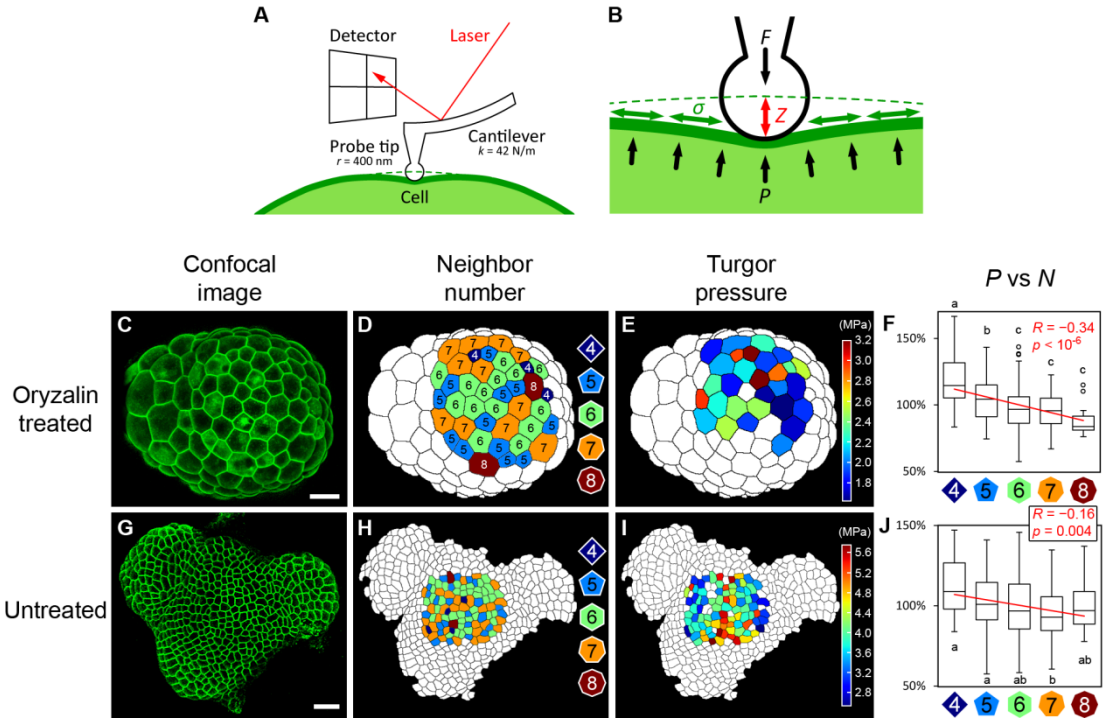


**Figure 1. Turgor pressure heterogeneity in SAM is associated with variation of cell topology.**

(**A** and **B**) Schematic representation of AFM nanoindentation for turgor pressure measurement. *r*, probe tip radius; *k*, cantilever stiffness; *F*, indentation force; *Z*, indentation depth; *P*, turgor pressure; *σ*, cell wall tension. (**C** to **J**) Cell-specific turgor pressure in oryzalin-treated (C to F) and untreated SAM (G to J). (C and G) Top-view surface projections of SAM, oryzalin-treated (C) or untreated (G), with plasma membrane GFP signal; scale bars represent 20 µm. (D and H) Cell topology determined on segmented cell contour images, around SAM center; numbers indicate neighbor number in epidermis. (E and I) AFM-determined cell-specific turgor pressure heat maps. (F and J) Box plots of cellular turgor pressure *P* normalized per SAM against cell topology *N* (F, oryzalin-treated 9 SAMs, $n = 202$ cells; J, untreated 5 SAMs, $n = 326$ cells). Circles are Tukey's outliers; lowercase letters indicate statistically different populations (Student's *t*-test, $p < 0.05$); red lines indicate linear regressions, with Pearson correlation coefficient *R* and corresponding *p*-value.

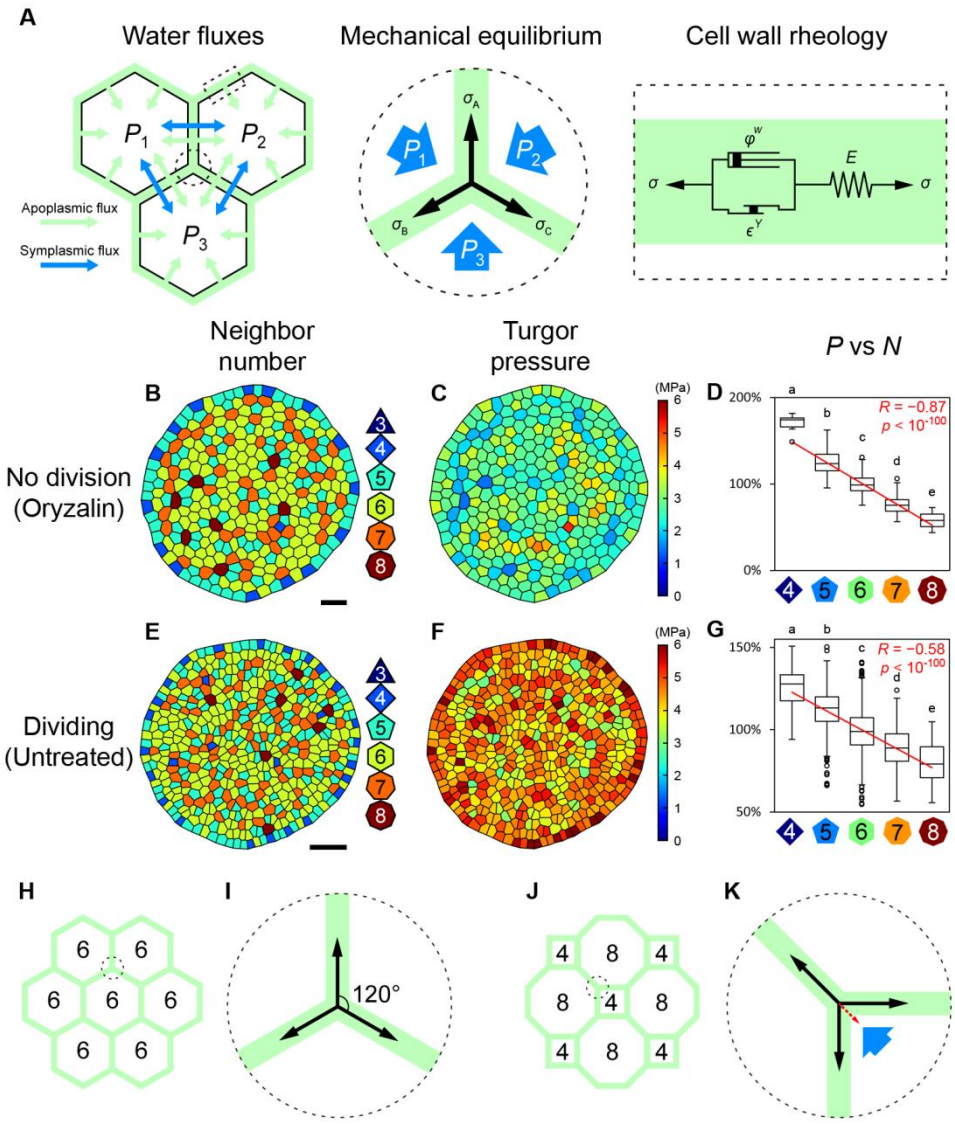


**Figure 2.Turgor pressure heterogeneity emerges from cell topology.**

(**A**) Schematic representations of model components, including apoplasmic and intercellular water fluxes (left), mechanical equilibrium at three-cell junctions (middle) and the visco-elasto-plastic cell wall rheology. *P*, cell-specific turgor pressure; $\sigma$, cell wall tension; $\varphi^w$, wall extensibility; $\epsilon^Y$, wall strain threshold; *E*, wall Young's modulus. (**B** to **G**) Turgor pressure in non-dividing (oryzalin-treated, B to D) and dividing (untreated) simulations (E to G), scale bars are 5 unit length. (B and E) Cell topology; (C and F) cellular turgor pressure heat maps; (D and G) Box plots of normalized cellular turgor pressure *P* against cell topology *N* (D, non-dividing 5 simulations, $n$ = 1219 cells; G, dividing 8 simulations, $n$ = 3240 cells). Cells on the mesh edge were not analyzed due to border effect. Circles are Tukey's outliers; lowercase letters indicate statistically different populations (Student's *t*-test, $p < 0.05$); red lines indicate linear regressions, with Pearson correlation coefficient *R* and corresponding *p*-value. (**H** to **K**) Schematic explanation of topology-derived turgor pressure heterogeneity. (H and I) Three-cell junctions in a tissue of hexagonal cells are at mechanical equilibrium with equal wall-wall angles. (J and K) Fewer-neighbored cells have sharper wall-wall angles, effectively resulting in mechanical compression due to unequal tension distribution (red dash-line arrow) that is balanced by higher turgor pressure buildup (big blue arrow).

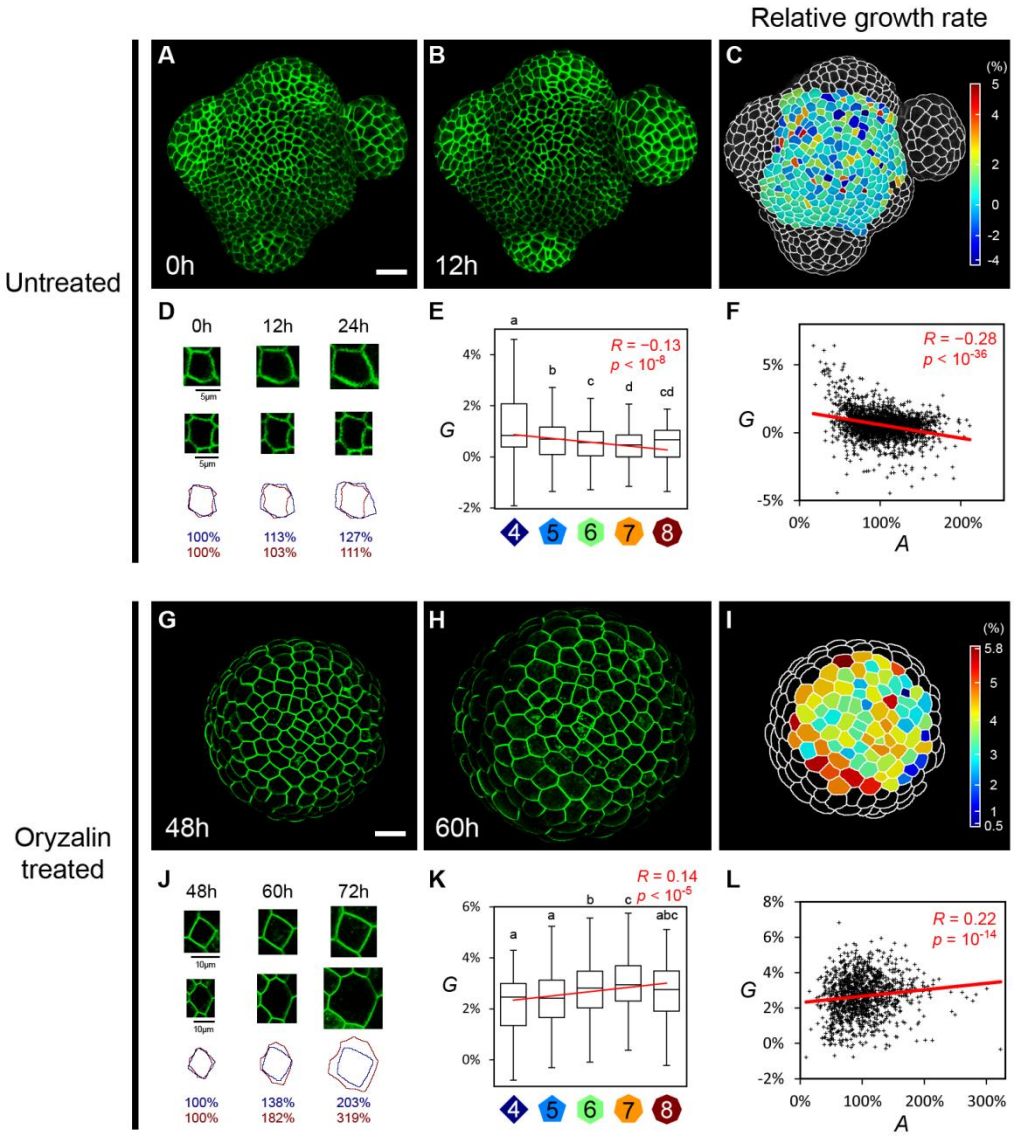


**Figure 3. Cellular growth rate bifurcates between conditions.**

(**A** to **F**) Relative growth rate per hour *G* of untreated SAM cells between 12-hour interval. (**G** to **L**) Cellular growth rate per hour of oryzalin-treated SAM between 12-hour interval (48 and 60 hours post treatment). (A, B, G and H) Surface projections of untreated or oryzalin-treated SAM at initial time point (A and G) and 12 hours later (B and H); scale bars are 20 µm unless otherwise noted. (C and I) Heat maps of areal relative growth rate per hour. Note that the color lookup tables are exponential. (D and J) Example 4 and 8-neighbored cells during 24-hour growth, with areal normalization at initial time point. Cell contour and relative size (blue for 4-neighbored, red for 8-neighbored) depict the diverging growth trends. Scale bars are as indicated. (E, F, K and L) Box plots of relative growth rate per hour *G* against cell topology *N* (E and K) and dot plots of relative growth rate per hour *G* against normalized cell area *A* (F and L) (E and F, untreated 11 SAMs, $n$ = 2013 cells; K and L, oryzalin-treated 14 SAMs, $n$ = 1160 cells). Note that Tukey's outliers are not plotted, but are included for statistical analyses. Lowercase letters indicate statistically different populations (Student's *t*-test, $p < 0.05$); red lines indicate linear regressions, with Pearson correlation coefficient *R* and corresponding *p*-value.

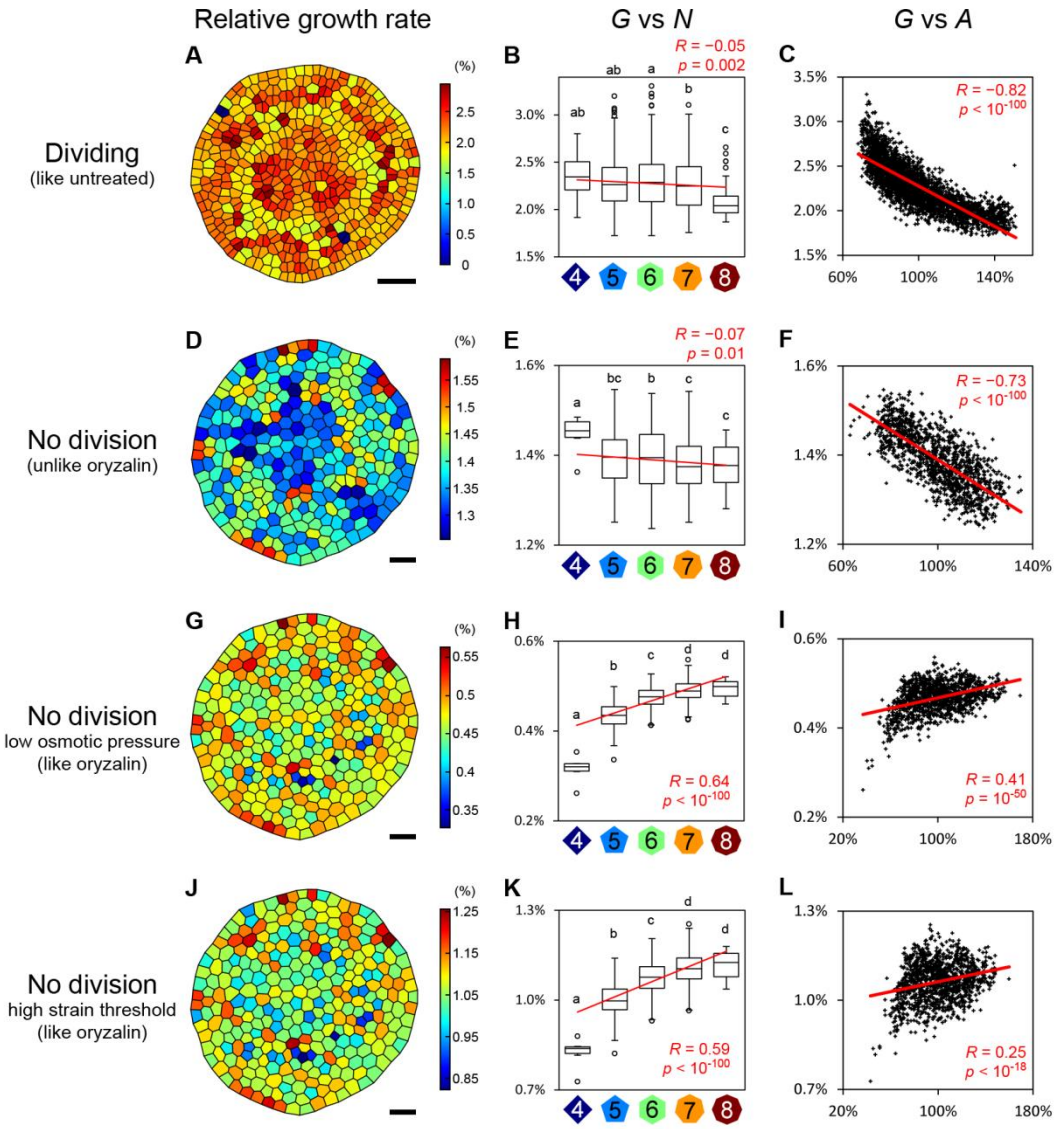


**Figure 4. Reducing osmotic pressure or increasing growth threshold invert growth trend.**

(**A** to **C**) Relative growth rate per hour *G* in simulations with cell division, which mimics untreated SAM. Cells that just divided (dark blue) are not included in analysis. (**D** to **F**) Growth simulations with no cell division to mimic oryzalin treatment. Growth does not recapitulate oryzalin-treated SAM. (**G** to **I**) Growth simulations with no division plus reduced osmotic pressure. Growth recapitulates oryzalin-treated SAM. (**J** to **L**) Growth simulations with no division plus elevated cell wall strain threshold. Growth also recapitulates oryzalin treatment. (A, D, G and J) Heat maps of areal relative growth rate per hour. Scale bars are 5 unit length. (B, E, H and K) Box plots of relative growth rate per hour *G* against cell topology *N* (B, dividing 8 simulations, $n$ = 3240 cells; E, H and K, non-dividing 5 simulations each, $n$ = 1219 cells). Lowercase letters indicate statistically different populations (Student's *t*-test, $p < 0.05$); red lines indicate linear regressions, with Pearson correlation coefficient $R$ and corresponding $p$-value. (C, F, I and L) Dot plots of relative growth rate per hour *G* against normalized cell area *A*.